Article

Optical Spectra of Delocalized Dinitroaromatic Radical Anions Revisited

Stephen F. Nelsen, Michael N. Weaver, Jeffrey I. Zink, and Joo P. Telo

J. Am. Chem. Soc., **2005**, 127 (30), 10611-10622• DOI: 10.1021/ja051178u • Publication Date (Web): 12 July 2005

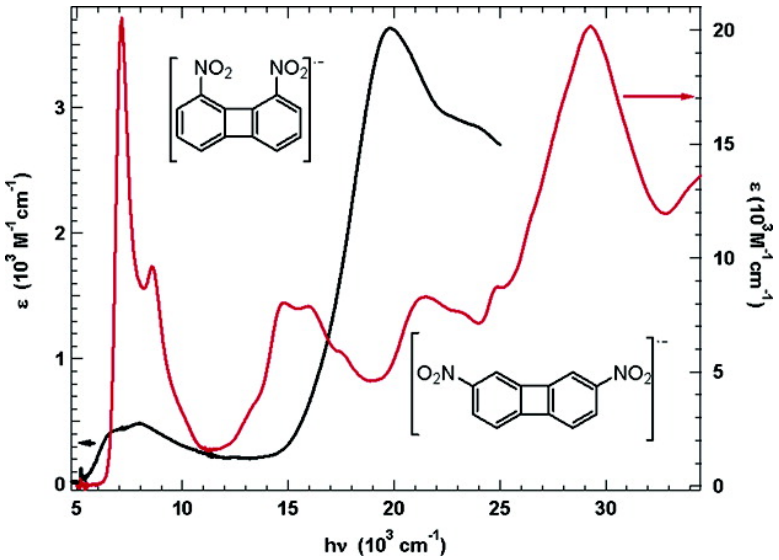

More About This Article

Additional resources and features associated with this article are available within the HTML version:

- Supporting Information
- Links to the 11 articles that cite this article, as of the time of this article download
- Access to high resolution figures
- Links to articles and content related to this article
- Copyright permission to reproduce figures and/or text from this article

View the Full Text HTML

J|A|C|S
ARTICLES
Published on Web 07/12/2005

Optical Spectra of Delocalized Dinitroaromatic Radical Anions Revisited

Stephen F. Nelsen,*,† Michael N. Weaver,† Jeffrey I. Zink,‡ and João P. Telo§

Contribution from the Department of Chemistry, University of Wisconsin, 1101 University Avenue, Madison, Wisconsin 53706-1396, Department of Chemistry and Biochemistry, University of California, Los Angeles, California 90095, and Instituto Superior Técnico, Química Orgânica, Av. Rovisco Pais, 1049-001 Lisbon, Portugal

Received February 24, 2005; E-mail: nelsen@chem.wisc.edu

Abstract: The optical spectra of nine dinitroaromatic radical anions (1,2- and 1,4-dinitrobenzene, 1,5- and 2,6-dinitro naphthalene, 4,4′-dinitrobiphenyl, 2,7-dinitro-9,9-dimethylfluorene, 2,6-dinitroanthracene, and 2,7- and 1,8-dinitrobiphenylene) in dimethylformamide are reported and analyzed. All have delocalized charge distribution, as demonstrated by the vibrational fine structure that is observed in their optical spectra: All show lowest energy absorption bands that correspond to an α-homo (highest occupied molecular orbital) to α-lumo (lowest unoccupied) transition, as shown by Koopmans-based UB3LYP calculation of the orbital separation of the neutral at the geometry of the radical anion. These single-point calculations are shown to be significantly more accurate for five of these compounds than the much more complex and expensive TD-DFT method. The two-state model should not be used to estimate the electronic coupling in delocalized intervalence compounds such as these. Neighboring orbital estimation of the electronic couplings show that using the two-state model greatly underestimates electronic coupling here.

Introduction

We recently reported the optical absorption spectra of the radical anions of the first six dinitroaromatics shown below.[1]

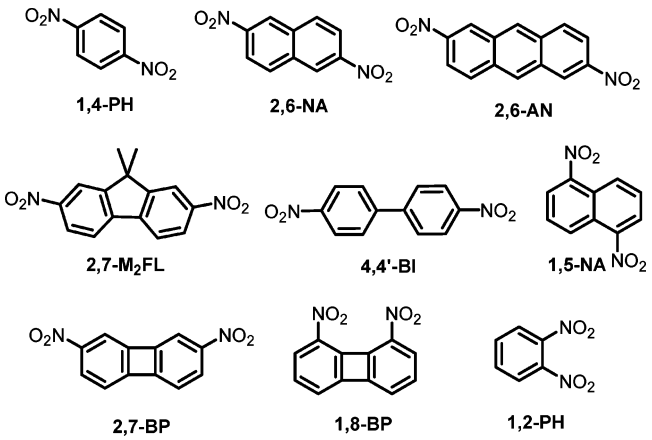

All are symmetrical intervalence compounds with delocalized charge. Symmetrical intervalence compounds have the same two formal "charge bearing units" **M** (the nitro groups for the present work) connected in a symmetrical manner to a bridge (**B**) and are at an oxidation level for which the **M** groups might have different charges. These compounds may thus be abbreviated $[\mathbf{M}-\mathbf{B}-\mathbf{M}]^-$. We analyzed these spectra using the usual Marcus−Hush two-state model,[2] for which the off-diagonal matrix coupling element (H_{ab}, also called the electronic coupling between the **M** groups) is simply half the transition energy for the first band maximum (E_{a1}). We also extracted the electron-transfer distance on the diabatic surfaces (d_{ab}) from the integrated band intensity, using the equation derived by Cave and Newton in their generalized Mulliken−Hush theory.[3] The quantities obtained had some odd aspects. There was considerable curvature in plots of $\log(H_{ab})$ versus the number of connecting bonds; **1,5-NA**$^-$ gave an H_{ab} that is closer to that expected for the eleven-bond longest pathway between the nitrogens than that of the shortest, five-bond pathway, making the usual statement that H_{ab} depends on distance between the charge-bearing units quite incorrect for this example; and the d_{ab} values obtained were remarkably small. The purpose of this paper is to point out that it is not reasonable to apply the two-state model to dinitroaromatic radical anions (or any other delocalized intervalence compounds of which we are aware), which is consistent with the anomalies pointed out above. We discuss here the origin of the first several optical absorption bands for the delocalized intervalence radical anions of the nine dinitroaromatic compounds shown above and how the position of these bands is related to electronic couplings in these systems.

† University of Wisconsin.
‡ University of California.
§ Instituto Superior Técnico.

(1) Nelsen, S. F.; Konradsson, A. E.; Weaver, M. N.; Telo, J. P. *J. Am. Chem. Soc.* **2003**, *125*, 12493−12501.

(2) For some older reviews, see: (a) Hush, N. S. *Prog. Inorg. Chem.* **1967**, *8*, 391. (b) Hush, N. S. *Coord. Chem. Rev.* **1985**, *64*, 135. (c) Marcus, R. A.; Sutin, N. *Biochim. Biophys. Acta* **1985**, *811*, 265−322. (d) Sutin, N. *Prog. Inorg. Chem.* **1983**, *30*, 441−499.

(3) (a) Cave, R. J.; Newton, M. D. *J. Chem. Phys.* **1997**, *106*, 9213. (b) Obtained from $|\Delta\mu_{ab}| = [(\Delta\mu_{12})^2 + 4(\mu_{12})^2]^{1/2}$ using $\Delta\mu$ (D) = 4.8032 d (Å). $\Delta\mu_{12} = 0$ for a delocalized compound, so d_{ab} may be obtained directly from the transition dipole moment, μ_{12}.

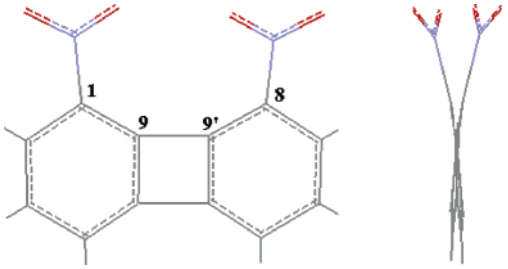

Figure 1. Two views of the calculated structure of **1,8-BP**$^-$.

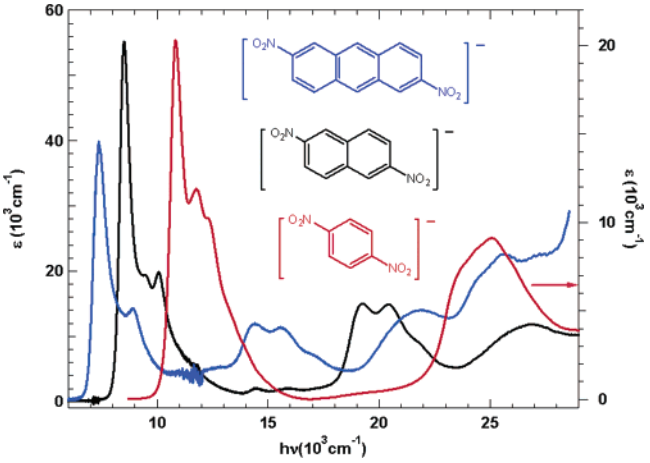

Figure 2. Optical spectra of **1,4-PH**$^-$, **2,6-NA**$^-$, and **2,6-AN**$^-$ in DMF.

Results

1,8-Dinitrobiphenylene (**1,8-BP**) is a new compound, prepared by an Ullman coupling similar to that used for the previously known **2,7-BP** (see Experimental Section). **1,8-BP** was prepared to provide an example of a dinitro radical anion with Ar−NO_2 bonds that are nearly parallel. All of the others studied here have angles between their **B-M** bonds that are greater than 90°, as do almost all intervalence compounds ever studied. UB3LYP/6-31G* calculations on its radical anion give a C_2 twisted structure (see Figure 1) that is 1.4 kcal/mol more stable than the untwisted C_{2v} structure. The nitro groups are significantly twisted, with a C_2C_1,NO twist angle of 17.2° and C_9C_1,NO′ twist angle of 13.0°, corresponding to a nitrogen p orbital, C_1 p orbital twist of 15.1°. Twist across the center of the molecule, C_1C_9,$C_9'C_8$ is 6.1°, and the NC_1,C_8N' twist angle is 27.7°.

The optical spectra of these radical anions in DMF at room temperature are shown in Figures 2−6, and the peak positions are summarized in Table 1. The lowest energy absorption band is designated E_{a1}. In addition to the lowest energy bands that show partially resolved vibrational fine structure and that were previously examined,[1] a variety of other bands are observed below about 30 000 cm^{-1}. This paper is concerned with the origin of these lower energy bands and how they should be interpreted in terms of electronic coupling. It may be noted that the lowest energy band maximum (E_{a1}) values for the three compounds not previously discussed are all anomalous in terms of the two-state model. E_{a1} is nearly the same for the 5-bond **1,8-BP**$^-$ as the 7-bond **2,7-BP**$^-$, and the 3-bond **1,2-PH**$^-$ has a lower E_{a1} than that of the 5-bond **1,4-PH**$^-$. The previously unknown biphenylene radical anions were characterized by EPR (see Experimental Section).

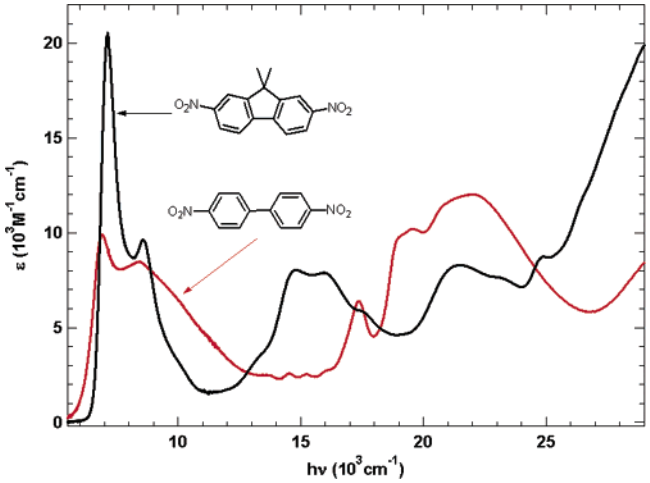

Figure 3. Optical spectra of **2,7-M$_2$FL**$^-$ and **4,4′-BI**$^-$ in DMF.

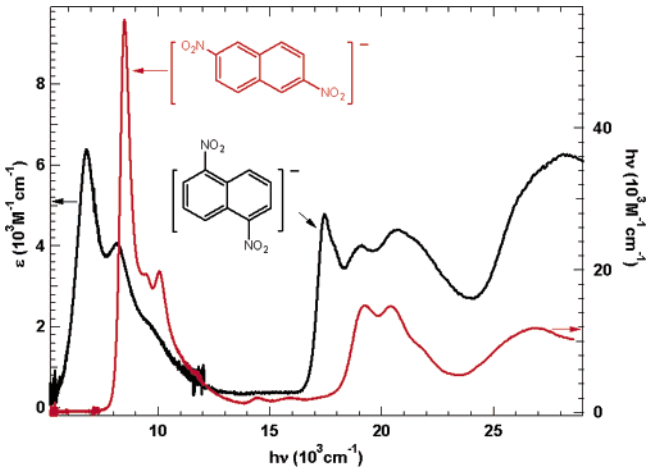

Figure 4. Optical spectra of **1,5-NA**$^-$ and **2,6-NA**$^-$ in DMF.

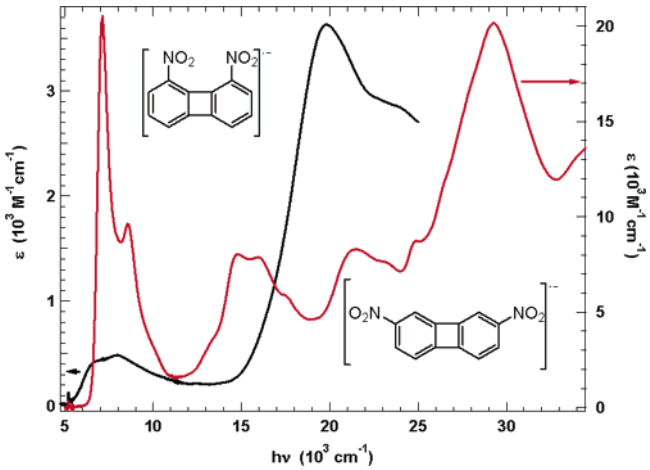

Figure 5. Optical spectra of **1,8-BP**$^-$ and **2,7-BP**$^-$ in DMF.

Discussion

Band Assignments. Optical transitions in doublet systems are often discussed in terms of a restricted open-shell (also called half-electron)[4] model, where all the orbitals are doubly occupied except for one singly occupied one (which we will call the *SOMO*). This leads to orbital diagrams such as those shown in

(4) Clark, T. *A Handbook of Computational Chemistry*; Wiley: New York, 1985; p 97.

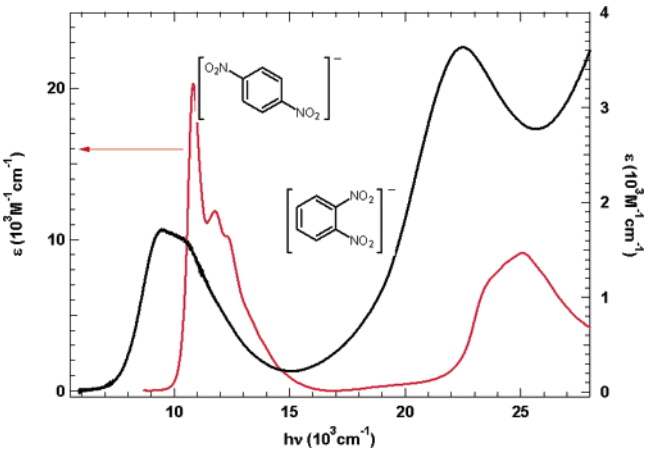

Figure 6. Optical spectra of **1,2-PH**$^-$ and **1,4-PH**$^-$ in DMF.

Table 1. Comparison of Observed and Calculated[a] Band Maxima for Dinitroaromatics

species	E_{a1}(obs) (cm^{-1})	B_1 (cm^{-1})	other E_a(obs) (cm^{-1})	other calculated bands (cm^{-1})
1,2-PH$^-$	9440	10 160	22 470	B_2: 21 670
			30 120	A_3: 27 960, A_4: 30 310
1,4-PH$^-$	10 820	11 770	23 700	B_2:20 440[20 790][a]
		[11 150][a]		A_2:26 740[26 350][a]
2,6-NA$^-$	8500	9060	19 250	A_1: 23 620[22 600]
		[8450]		
2,6-AN$^-$	7380	7960	14 400	A_1: 17 650
1,5-NA$^-$	6750	7360	17 440	A_1: 21 620[20 570]
		[7160]	~19 000,~20 500	
4,4′-BI$^-$	6900	6740	(17 400)	B_2: 17 620
			~19 600, ~22 000+	B_3: 19 710, A_1: 24 260
2,7-M$_2$FL$^-$	6780	6870	18 970	B_2: 17 200, A_1: 23 570
			20 600	
1,8-BP$^-$	6800	7300	19 800	B_3: 20 970, A_1: 20 570
	7840	8400		
2,7-BP$^-$	7072	7910	14 800	A_1: 17 320
			21 500	B_3: 19 390

[a] Koopmans-based calculations at the B3LYP/6-31G* level [in brackets, B3LYP/6-31+G* level]. See Band Assignments section for description of Koopmans-based calculations.

Figure 7.[5] Stable neutral compounds typically have a bigger gap between their highest occupied molecular orbital (*HOMO*) and lowest unoccupied one (*LUMO*) than between either filled or virtual orbitals. Removal of an electron then gives a cation radical with a *SOMO* closer to the filled orbitals than the virtual ones, as shown at the left of Figure 7, and the smallest excitation energies correspond to filled orbital to *SOMO* transitions, Type A, indicated as A_i in Figure 7. Addition of an electron populates the *LUMO* of the neutral species, and as indicated on the right of the diagram, and then the smallest excitation energies correspond to *SOMO* to virtual orbital transitions, type B, indicated as B_i in Figure 7. Because alternate aromatic hydrocarbons have virtual orbitals that are nearly paired in relative energy with the filled orbitals, the absorption spectra of their radical cations and radical anions are quite similar, as already pointed out by Hoijtink in 1957 discussing the spectrum from perylene in concentrated sulfuric acid as the radical cation because of its resemblance to that of the known radical anion.[6] Type A transitions are between configurations of the type ...-$(HOMO\text{-}1)^2(HOMO)^2(SOMO)^1 \rightarrow ...(HOMO\text{-}1)^2(HOMO)^1$-

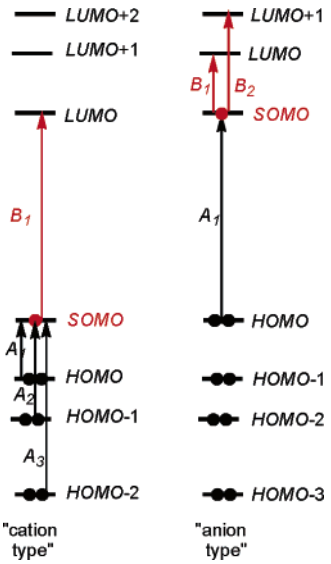

Figure 7. ROHF models of the orbital energies of doublet radicals, showing the Hoijtink type A and type B transitions.

$(SOMO)^2$ and are also called K (for Koopmans). The lowest energy type B transition is between configurations ...$(HOMO\text{-}1)^2(HOMO)^2(SOMO)^1 \rightarrow ...(HOMO\text{-}1)^2\ (HOMO)^2(SOMO)^0(LUMO)^1$ and is also called NK (non-Koopmans). There are, however, actually no two electron orbitals in a doublet species. All of the orbitals of a radical ion are actually split into α and β spin sets, and electronic excitation does not flip spins, so the type A transitions are $\beta(HOMO)\rightarrow\beta(LUMO)$, $\beta(HOMO\text{-}1)\rightarrow\beta(LUMO)$ etc. and the type B transitions are $\alpha(HOMO)\rightarrow\alpha(LUMO)$, $\alpha(HOMO)\rightarrow\alpha(LUMO{+}1)$, etc. More complex non-Koopmans' transitions also occur, such as type C, $\alpha(HOMO\text{-}n) \rightarrow \alpha(LUMO{+}n)$ or $\beta(HOMO\text{-}n)\rightarrow\beta(LUMO{+}n)$, as well as multiple electron excitations such as the superexchange transition of localized intervalence radical ions, which we suggest is most simply considered as a concerted double excitation $\mathbf{B^0\rightarrow M^+, M^0\rightarrow B^0}$ (for a radical cation) or $\mathbf{B^0\rightarrow M^0, M^-\rightarrow B^0}$ (for a radical anion).

TD-DFT calculations[7] indicate that the lower energy transitions for many delocalized intervalence radical ions, including the lower transitions of the dinitroaromatic radical anions studied here, are quite predominately either type A or B transitions. The results of TD-DFT calculations on 1,4-dinitrobenzene radical anion are shown in Table 2. As expected, the lowest energy transitions for dinitroaromatic radical anions are type B transitions. The first four transitions are calculated using TD-DFT to be predominately B_1, B_2, A_1, and A_2 transitions in that order, although three of the four are only 73−83% of such character. The fifth transition is calculated to be a serious mixture of A_5 and a type C transition. However, zero intensity is calculated for transitions 2−5, although transition 4 (A_2) is g→u and is not symmetry-forbidden. These calculations do not give even a qualitative description of the observed spectrum; the only band calculated to have observable intensity is calculated 3900 cm^{-1} too high in energy, and the second observed band is missed entirely.

(5) (a) Bally, T. In *Radical Ionic Systems*; Lund, A.; Shiotani, M., Eds.; Kluwer: Dortrecht, 1991; p 3. (b) Čársky, P.; Zahradník, R. *Top. Curr. Chem.* **1973**, *43*, 1.

(6) (a) Hoijtink, G. J.; Weijland, W. P. *Recl. Trav. Chim.* **1957**, *76*, 836. (b) Buschow, K. J. J.; Dieleman, J.; Hoijtink, G. J. *Mol. Phys.* **1963**−**1964**, *7*, 1.

(7) (a) Burke, K.; Gross, E. K. U. A Guided Tour of Time-Dependent Density Functional Theory. In *Density Functionals: Theory and Applications*; Joubert, D., Ed.; Springer: Berlin, 1998; pp 116−146. (b) Casida, M. E.; Jamorski, C.; Casida, K. C.; Salhub, D. R. *J. Chem. Phys.* **1998**, *108*, 4439−4449. (c) Stratmann, R. E.; Scuseria, G. E.; Frisch, M. J. *J. Chem. Phys. Chem.* **1998**, *109*, 8218−8224.

Table 2. Comparison of TD-DFT and Koopmans-Based Calculations[a] of the Optical Spectrum of 1,4-Dinitrobenzene Radical Anion (**1,4-PH**$^-$)

	TD-DFT calcn		NAG/DAG calcn
ex	$h\nu$(cm^{-1})(f)	assignment	assignment: $h\nu$(cm^{-1}) (f)
1	14 720 (0.21)	73% 44α→45α(B_1) 13% 41β→44β(A_3) 1% 40β→46β(C)	B_1: 11 150(0.19) [11 765]
2	19 920 (0.00)	100% 44α→46α(B_2) 1% 41α→45α(C) 1% 40β→45β(C)	B_2: 20 790(0.00) [20442]
3	23 130 (0.00)	83% 43β→44β(A_1) 15% 42β→45β(C) 4% 42α→45α(C)	A_1: 25 360(0.00) [25 660]
4	23 710 (0.00)	78% 42β→44β(A_2) 6% 43α→45α(C) 1% 42β→51β(C) 1% 42α→45α(C)	A_2: 26 350(0.00) [26 740]
5	25 390 (0.00)	65% 39β→44β(A_5) 29% 36α→45α(C) 33% 4×C	A_3: 27 470 (0.14) A_4: 28 660 (0.00) A_5: 30 780 (0.00)

[a] Calculated at the UB3LYP/6-31+G* geometry, with UB3LYP/6-31G* transition energies shown in brackets for the Koopmans-based calculations.

We introduced a simpler method for estimating the Hoijtink type A transition energies for radical cations using the "neutral in cation geometry" (NCG) method, in which a single point at the geometry of the radical cation is calculated with a neutral charge, so the system is closed-shell, and the orbitals involved in the transitions each have two electrons.[8] The equal orbital occupancy allows Koopmans' theorem,[9] that ionization potentials may be equated with the negative of orbital energies,[5a] to work quite well. The orbital separation in an NCG radical cation calculation is a good approximation to the transition energy that would be calculated by a more sophisticated method, and even simple semiempirical calculations proved useful for understanding experimental data.[10] Not surprisingly, single-point NCG calculations using UB3LYP/6-31G* geometry (which we will call DFT calculations for brevity) structures give answers closer to experiment than do the AM1 calculations,[11] and we only use numbers obtained from DFT-optimized radical ion geometries here.[12] Calculation of Type A transitions for a radical anion requires "dianion in anion geometry" (DAG); the Koopmans-based A_1 transition energy is the energy difference between the *homo* and the *homo*-1 orbitals, and so forth. We recently pointed out that the correspondingly simple estimate of type B transition energies is to use orbital energy separations for the neutral at anion geometry (NAG) for radical anions.[13] The B_1 transition energy is the difference in energy between the *lumo* and *lumo*+1 for the NAG calculation. This results in no electrons in either orbital for the B transitions, and Koopmans' theorem works as well as it does for type A transitions in many cases. The intensities of NAG and DAG transitions may be obtained from the dipole matrices, which may be printed using the Weinhold Natural Bond Orbital program keyword "DIMO",[14] and the oscillator strengths obtained from them are included in Table 2 above.[15] Table 2 compares the TD-DFT calculations with the Koopmans-based calculations for **1,4-PH**$^-$, and Figure 8 compares them graphically. The orbital energies are considerably changed between the open-shell DFT calculation used for the TD-DFT and the far less expensive closed-shell Koopmans-based calculations. The intense A_3 band that is the principal contributor to the second large band in the spectrum happened not to lie in the first five transitions that TD-DFT calculated (from comparison with other compounds we have studied we would expect the TD-DFT A_3 band to lie a few thousand wavenumbers higher in energy than the DAG estimate). Since no configuration interaction is used, interpretation is much simpler for the Koopmans-based calculations. The Koopmans-based transition energies are often closer to experimental ones than when using TD-DFT, and the intensities are rather similar to TD-DFT calculations of transitions that are predominately either the Type A or B ones that NAG/DAG treats. Other types of transitions are often present in radical ion spectra,[5a] but Koopmans-based calculations do not address them. Figures 9−12 show similar TD-DFT, Koopmans-based optical spectrum comparisons for **1,5-NA**$^-$ and **2,6-NA**$^-$ and also **1,8-** and **2,7-BP-** (For the data plotted, and comparison of 6-31+G* and 6-31G* basis set data for the naphthalene derivatives, see the Supporting Information). In these cases as well, the lowest energy transition is clearly B_1, and NAG calculations do a better job of predicting the transition energy than do TD-DFT calculations. The next lowest energy bands are Type A transitions for three of the four compounds, but a rather strong type B transition contributes to the band about at about 30 000 cm^{-1} for **1,5-NA**$^-$. Figures 13 and 14 show the observed and predicted B_1 bands for the three benzenoid aromatics and the two biphenylene derivatives, respectively, using the same ϵ and oscillator strength (f) scales on each graph. The calculated f values are in the order of the ϵ_{max} values, but the drop-off in experimental ϵ_{max} values is considerably larger than that in calculated f. The f values would only have a linear correlation with ϵ_{max} if the bandwidths were the same, and the bandwidth is clearly broader for **1,5-NA**$^-$ than for **2,6-NA**$^-$ < **1,4-PH**$^-$ (bandwidth estimates (Γ) based upon simulation of band structure are **1,4-PH**$^-$ 556 cm^{-1}, **2,6-NA**$^-$ 506 cm^{-1}, **1,5-NA**$^-$ 994−1016 cm^{-1}).[1] The B_1 band of **^{18}BP**$^-$ is obviously significantly broader than that of **^{27}BP**, and the ϵ_{max} ratio here is considerably larger (Figure 14). We conclude that the oscillator strengths correlate qualitatively rather well with the observed data.

The Koopmans-based calculations allow explicit pictures of what orbitals are involved. Figure 15 shows orbital density drawings for **1,4-PH**$^-$ displayed next to NAG/DAG energy levels that represent transition energies relative to the SOMO, orbital 44 (B_{3u} in D_{2h} symmetry). Orbitals 43 and 42 are both oxygen p-lone pair combinations that have vanishing overlap

(8) (a) Nelsen, S. F.; Blackstock, S. C.; Yumibe, N. P.; Frigo, T. B.; Carpenter, J. E.; Weinhold, F. *J. Am. Chem. Soc.* **1985**, *107*, 143−149. (b) Clark, T.; Teasley, M. F.; Nelsen, S. F.; Wynberg, H. *J. Am. Chem. Soc.* **1987**, *109*, 5719−5724.
(9) Koopmans, T. *Physica* **1934**, *1*, 104.
(10) Nelsen, S. F.; Tran, H. Q.; Nagy, M. A. *J. Am. Chem. Soc.* **1998**, *120*, 298−304.
(11) Nelsen, S. F.; Luo, Y.; Weaver, M. N.; Zink, J. I. "Beyond the Two-State model: Optical Spectra of Protected Diamine Intervalence Radical Cations Related to *N*,*N*,*N*′,*N*′-Tetraalkylbenzidine", to be published.
(12) It is worth noting here that Koopmans-based HF calculations, despite having better geometries, are not nearly as useful for predicting optical spectra as AM1 calculations, presumably because they lack any electron correlation.
(13) Nelsen, S. F.; Konradsson, A. E.; Telo, J. *J. Am. Chem. Soc* **2005**, *127*, 920−925.
(14) Glendening, J. K.; Badenhoop, A. E.; Reed, J. E.; Carpenter, J. A.; Bohmann; Morales, C. M.; Weinhold, F. *NBO 5.0. E. D.* Theoretical Chemistry Institute, University of Wisconsin: Madison, WI, 2001.
(15) The dipole matrices contain the *x*, *y*, and *z* components of μ_{12} (in atomic units; 1 au = 2.5418 D, the unit preferred by chemists). We converted the μ_{12} (Debye) values thus obtained to oscillator strengths, f, using $f = 1.085 \times 10^{-5} E_a(\text{cm}^{-1})(\mu_{12}(\text{Debye})/4.8032)^2$.

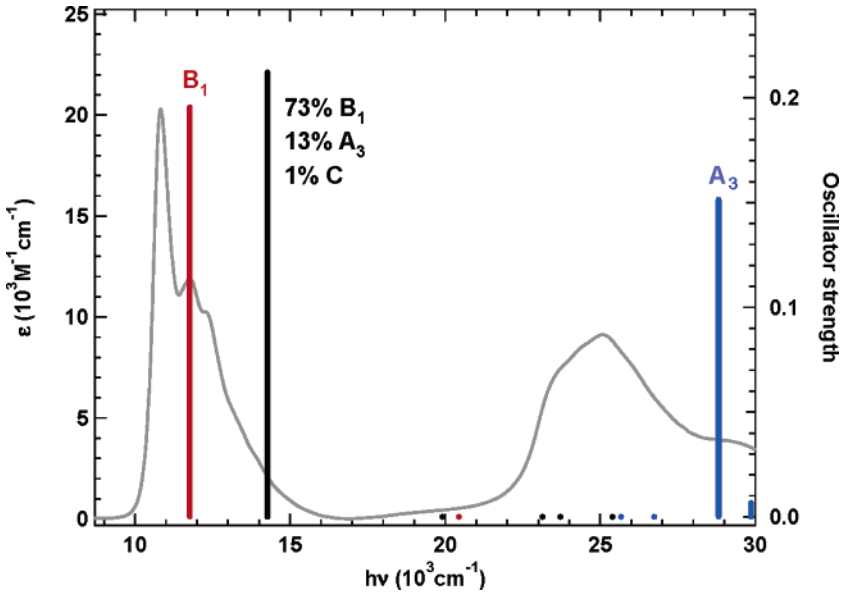

Figure 8. Comparison of TD-DFT (black sticks) with NAG (Type B, red sticks) and DAG (Type A, blue sticks) calculations of optical spectra for **1,4-PH**$^-$.

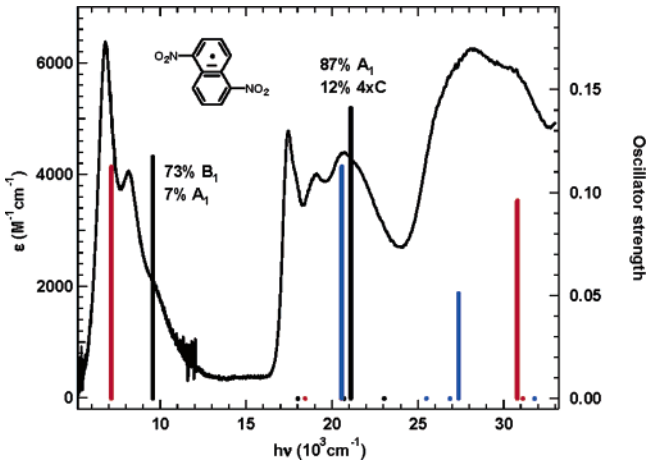

Figure 9. Comparison of TD-DFT (black sticks) with NAG (Type B, red sticks) and DAG (Type A, blue sticks) calculations of optical spectra for **1,5-NA**$^-$.

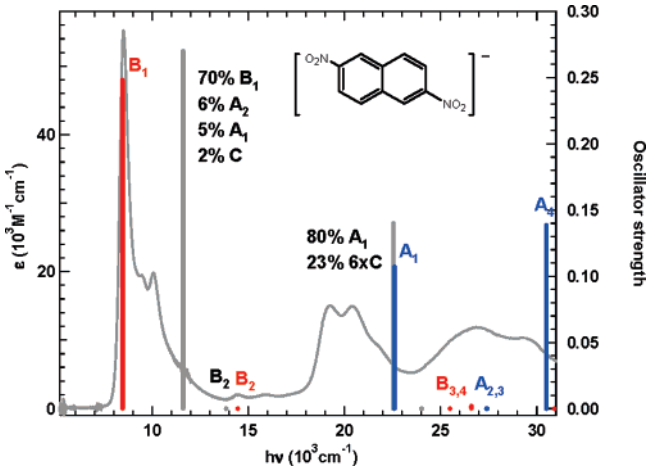

Figure 10. Comparison of TD-DFT (black sticks) with NAG (Type B, red sticks) and DAG (Type A, blue sticks) calculations of optical spectra for **2,6-NA**$^-$.

with the perpendicular C,N,O π-centered orbital 44, so the intensities of both the A_1 and A_2 transitions are zero, even

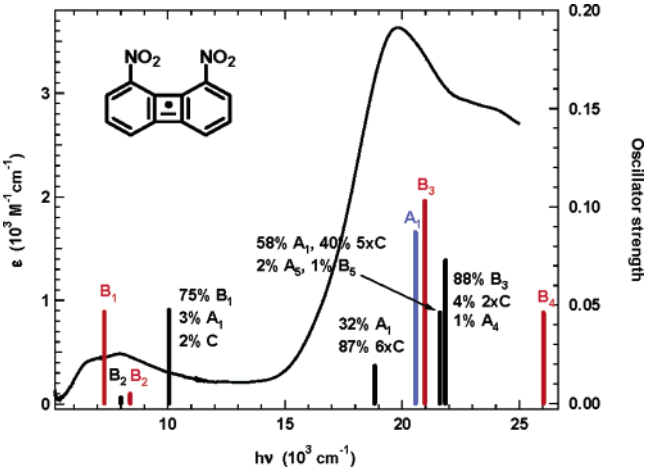

Figure 11. Comparison of TD-DFT (black sticks) with NAG (Type B, red sticks) and DAG (Type A, blue sticks) calculations of optical spectra for **1,8-BP**$^-$.

though orbital 42 has gerade symmetry so its transition to orbital 44 is not symmetry forbidden. The B_1 transition is clearly the partly resolved strong band observed at 10 820 cm^{-1}, and A_3 is presumably the major contributor to the broader band at 27 700 cm^{-1}.

Diffuse functions might be expected to be important for radicals, especially for radical anions. However, as is shown in Table 2 for **1,4-PH**$^-$ and is also true for **2,6-NA**$^-$ and **1,5-NA**$^-$, the difference between using 6-31G* and the 6-31+G* basis set that includes diffuse functions for estimating the transition energies proves to be small compared to any reasonable estimate of the error in such calculations (the changes upon going to the higher basis set are −620, +350, −300, −390, and +280 cm^{-1} for the five transitions of **1,4-PH**$^-$ shown in Table 2 and −610 and −200 cm^{-1} for the B_1 transitions of **2,6-NA**$^-$ and **1,5-NA**$^-$). It appears that nothing significant is actually gained by using a larger basis set for these compounds, and we have only used the computationally less expensive 6-31G* basis set for the other compounds. The lower energy Koopmans-based calculations for all nine of the delocalized dinitroaromatic radical anions are summarized in Table 1. The lowest energy transitions are all

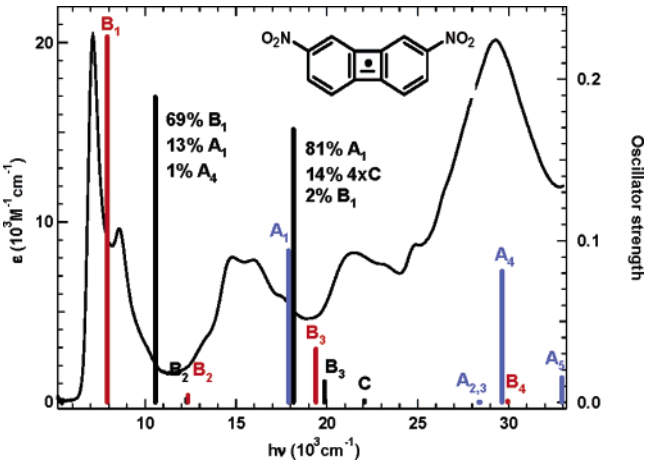

Figure 12. Comparison of TD-DFT (black sticks) with NAG (Type B, red sticks) and DAG (Type A, blue sticks) calculations of optical spectra for **2,7-BP**$^-$.

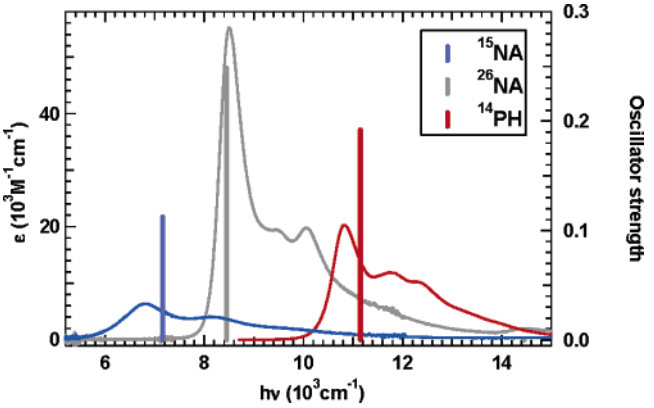

Figure 13. Comparison of observed and calculated B_1 bands for **1,4-NA**$^-$, **1,5-NA**$^-$, and **2,6-NA**$^-$.

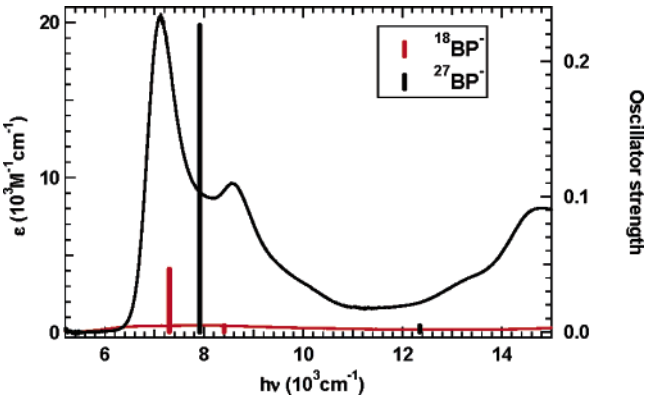

Figure 14. Comparison of observed and calculated B_1 bands for **1,8-BP**$^-$ and **2,7-BP**$^-$.

B_1, as indicated by the plot of calculated B_1 transition energy versus observed E_{a1} shown in Figure 16. The line shown has a slope of 1 and lies 600 cm^{-1} higher on the *y* (calculated) axis than the *x* (observed) axis. The calculated value for **4,4′-BI**$^-$ deviates the most from the experimental one, but the extremely facile twist at its central bond affects the calculated value substantially: constraining the central bond to 0° twist raises the B_1 transition energy by 335 cm^{-1}, but only increases the energy by 0.24 kcal/mol. The data for **1,2-PH**$^-$ (E_{a1} = 9440 cm^{-1}, d_{NN} = 3.07 Å) and **1,4-PH**$^-$ (E_{a1} = 10820 cm^{-1}, d_{NN} = 5.62 Å) make it quite clear that the two-state model prediction

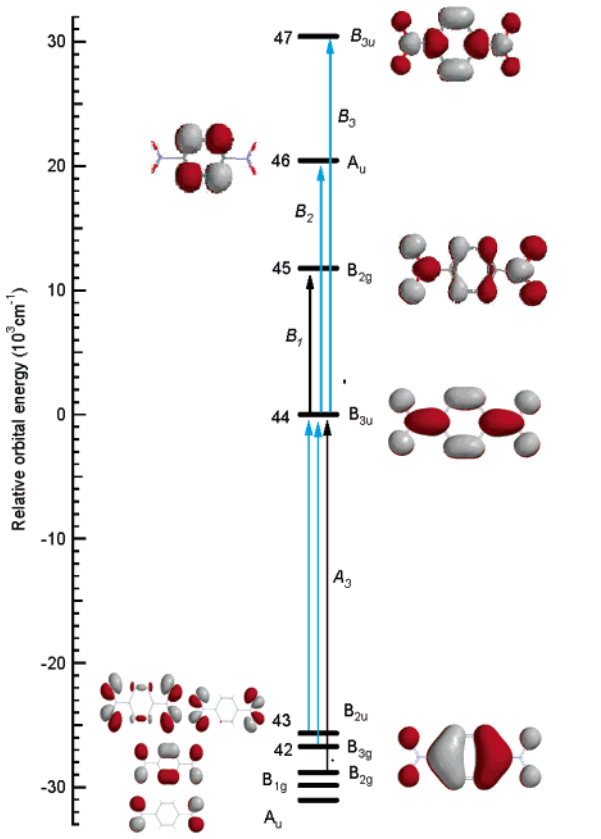

Figure 15. NAG/DAG transition energies and orbital density diagrams for the UB3LYP/6-31G* calculation on **1,4-PH**$^-$ (D_{2h} symmetry). Forbidden transitions are shown in blue.

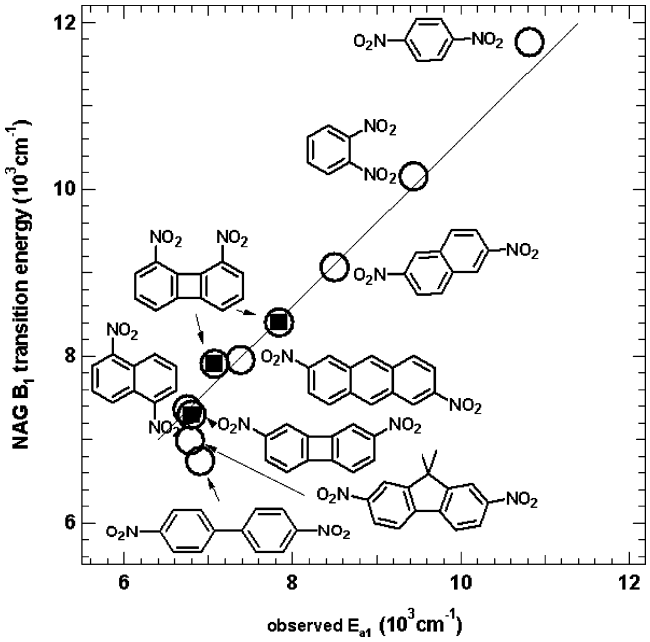

Figure 16. NAG-calculated B_1 transition energy versus observed peak maximum (E_{a1}). The data for the biphenylene-bridged compounds are marked with squares.

that E_{a1} will decrease logarithmically with increasing distance between the formally charge-bearing NO_2 groups is incorrect. **1,2-PH**$^-$ is calculated to be twisted, and the calculated p-orbital twist angle ϕ about the N−C bonds is 21.7° (cos ϕ = 0.93) and about the C_1C_2 bond is 28.0° (cos ϕ = 0.88), so it could be argued that, in the absence of the twisting, E_{a1} would be about

12 200 cm^{-1} for **1,2-PH**$^-$, which is larger than that for **1,4-PH**$^-$, but clearly less than expected for a distance only 55% as large.

The data for the biphenylene-bridged compounds are marked with squares, because these bridges are somewhat different than the linear arene and biphenyl-based aromatic bridges of the other compounds. The 2,7-substituted biphenylene radical anion **2,7-BP**$^-$ is delocalized, in contrast to the 2,7-disubstituted naphthalene, which is charge-localized, so its lowest optical transition is of completely different character than that for these delocalized compounds and is therefore discussed elsewhere.[16] The E_{a1} value for **2,7-BP**$^-$ is about the same as those for the **1,5-NA**$^-$, **2,7-M$_2$FL**$^-$, and **4,4′-BI**$^-$ examples, making it clear that distance between the nitro groups is hardly the only thing that determines E_{a1}; the N,N distances are calculated to be 8.72, 6.35, 9.70, and 9.99 Å, respectively. Furthermore, **1,8-BP**$^-$ (N,N distance 4.54 Å) shows two rather closely spaced transitions (the band shape is inconsistent with the two peaks observed being caused by vibrational fine structure for a single transition). The E_{a1} values are both smaller than that for the 9-bond bridged **2,6-AN**$^-$, again inconsistent with E_{a1} being directly related to electronic coupling that depends logarithmically upon distance between the charge-bearing units. Only **1,8-BP**$^-$ of the compounds studied is calculated to have two allowed bands in this region, and we suggest that calculating their position as well as for the other compounds is an impressive demonstration of the utility of NAG calculations for considering type B transition energies in radical anions. Both TD-DFT and NAG/DAG calculations predict the deviant behavior of the spectrum of **1,8-BP**$^-$, two low energy type B bands that are less intense than the second major absorption region (~20 000 cm^{-1}), which both calculations predict consists of both type A and B bands. Nevertheless, the NAG calculations appear more satisfactory; the intensities of the lowest energy bands are reversed in the TD-DFT calculation, and although the low energy band is predicted to be larger relative to the band ~20 000 cm^{-1} than observed by NAG/DAG, the TD-DFT intensity prediction is even further off. It does seem likely that the type C band obtained by TD-DFT contributes to the broad rise of the spectrum between 15 000 cm^{-1} and the maximum at about 20 000 cm^{-1}.

Neighboring Orbital Model. We will next consider the size of the electronic coupling for these molecules. The two-state model as applied to a delocalized intervalence compound (see Figure 17) considers only diabatic charge-bearing unit orbitals that are antisymmetric with respect to the plane bisecting a symmetrical intervalence compound, because they are the ones of interest for exchanging an electron between the charge-bearing units. This model is remarkably quantitatively successful for localized intervalence compounds[2,17] and intermolecular electron-transfer reactions.[2,18] However, there is a problem in applying this simple model to compounds that have such large H_{ab} that they are delocalized. Delocalized molecules actually are symmetric, so the molecular orbitals involving **M**, **B** mixing are combinations of the bridge and charge-bearing unit orbitals that are either symmetric or antisymmetric with respect to the

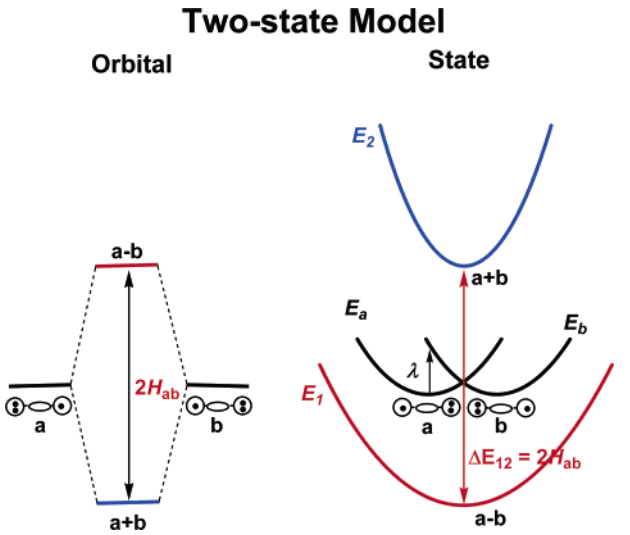

Figure 17. Cartoon representation of orbital and state diagrams using the two-state model for a case with large H_{ab} so the ground state (shown in red) is delocalized.

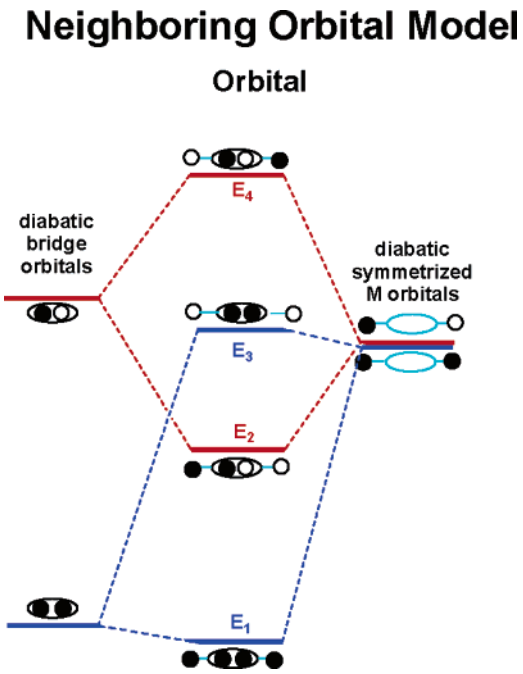

Figure 18. Orbital interaction diagram for a delocalized intervalence compound for which a single symmetric and a destabilized antisymmetric bridge orbital interacts with the charge-bearing unit symmetric and antisymmetric orbitals.

symmetry element at the center of the molecule. The diabatic charge-bearing unit orbitals (**M**) will occur in a symmetric and antisymmetric pair at the same energy (E_M) if there is no direct overlap between them. They will mix as separate two-state systems with symmetric and antisymmetric bridge orbitals, as indicated in the neighboring orbital model in Figure 18, which we have also used for an *N*,*N*′-diphenyl-hydrazine radical cation (where the bridge bears the charge and the M groups are phenyl rings)[19] and the **M** = **R$_2$N** aromatic-bridged radical cations.[11] The largest mixing will occur for the orbitals with the smallest diabatic energy gaps, leading to four adiabatic **M**,**B** combination orbitals, shown as E_1 to E_4 in Figure 18. For convenience, we

(16) Nelsen, S. F.; Weaver, M. N.; Konradsson, A. E.; Telo, J. P.; Clark, T. *J. Am. Chem. Soc.* **2004**, *126*, 15431−15438.
(17) Nelsen, S. F.; Ismagilov, R. F.; Trieber, D. A., II. *Science* **1997**, *278*, 846−849.
(18) Nelsen, S. F.; Pladziewicz, J. R. *Acc. Chem. Res.* **2002**, *35*, 247−254.
(19) Lockard, J. V.; Zink, J. I.; Trieber, D. A., II; Konradsson, A. E.; Weaver, M. N.; Nelsen, S. F. *J. Phys. Chem. A* **2005**, *109*, 1205−1215.

Table 3. Neighboring Orbital Solutions in cm^{-1} at $|R| = 1$ for Dinitroaromatic Radical Anions

bridge	E_4	E_3	E_2	E_1	ΔE^L	ΔE^U	V^U	V^L	H_{bb}	H^U	H^L	$H^U - H^L$
1,4-PH$^-$	30 415	11 765	≡0	−28 815	40 230	7240	14 770	2660	11 590	18 830	−28 640	47 470
1,2-PH$^-$	23 876	21 760	10 156	≡0	**−1290**	**13 560**	**1030**	**10 860**	**10 230**	**23 800**	**11 530**	12 270
					4200	8080	5550	8080	12 980	21 050	8780	
					21 310	−9043	5160	2190	21 540	12 490	220	
4,4′-BI$^-$	31 973	19 715	6744	≡0	**−5840**	**24 840**	**2210**	**9420**	**6940**	**31 780**	**11 630**	19 000
					11 380	7620	12 030	8050	15 550	23 170	4170	
					19 690	−690	12 610	440	19 700	19 010	10	
2,7-FLMe$_2$$^-$	32 757	20 263	6988	≡0	**−5890**	**25 370**	**2250**	**9690**	**7190**	**32 560**	**13 080**	19 480
					11 620	7860	12 270	8300	15 940	23 800	4320	
					20 240	−760	12 880	480	20 250	19 490	10	
1,5-NA$^-$	3179	20 633	7359	≡0	**−5500**	**24 200**	**2260**	**9940**	**7570**	**31 770**	**13 060**	18 710
					10 630	8080	11 630	8840	−1563	23 710	5000	
					20 400	−1810	12 280	1080	20 580	18 760	60	
2,6-NA$^-$	27 931	25 667	9064	≡0	**−5620**	**16 940**	**4150**	**12 520**	**10 030**	**26 970**	**15640**	11 150
					4660	−667	8830	12 620	15 160	21 830	10 500	
					24 630	−13 300	6690	3610	25 150	11 845	520	
2,6-AN$^-$	23 194	23 093	7955	≡0	**−4700**	**12 760**	**4170**	**11 300**	**9200**	**21 950**	**13 900**	8050
					3110	4940	7200	11 440	13 100	18 045	9990	
					23 020	−14 960	1450	940	23 060	8090	40	
1,8-BP$^-$	32 208	20 966	7295	≡0	**−5900**	**24 440**	**2430**	**10 060**	**7530**	**31 970**	**13 430**	18 540
					10 470	8080	11 790	9080	15 720	23 790	5250	
					20 790	−2260	12 410	1350	20 880	18 620	90	
2,7-BP$^-$	33 298	19 387	7909	≡0	**−3440**	**25 260**	**1300**	**9540**	**7980**	**33 230**	**11 410**	21 820
					14 060	7760	12 090	6680	16 720	24 490	2660	
					19 030	2890	12 620	1850	19 210	22 000	180	

will call the two electronic couplings in the neighboring orbital model V^U and V^L (instead of modifications of the H_{ab} that was traditional for the two-state model). The drawing has been made for a case with the symmetrized **M** diabatic orbitals lying between the bridge orbitals in energy, but closer to the antisymmetric upper bridge orbital, so that the electronic interaction between the lower **B** and **M** orbitals, V^L, is smaller than is V^U, because electronic couplings are proportional to $1/\Delta E$. *S* bridge orbitals can only mix with *S* **M** orbitals and *A* with *A*, so the Hamiltonian consists of two noninteracting but overlapping two-state models, see eq 1:

$$\begin{vmatrix} H_{aa} - E & V^U & 0 & 0 \\ V^U & H_{bb} - E & 0 & 0 \\ 0 & 0 & H_{bb} - E & V^L \\ 0 & 0 & V^L & H_{cc} - E = 0 \end{vmatrix} \quad (1)$$

The solutions for two-state equations are well-known,[20] leading to eqs 2−5 for the adiabatic surfaces in the neighboring orbital model:

$$E_1 = {}^1/_2(H^L + H_{bb} - [(\Delta E^L)^2 + 4(V^L)^2]^{1/2}) \quad (2)$$

$$E_3 = {}^1/_2(H^L + H_{bb} + [(\Delta E^L)^2 + 4(V^L)^2]^{1/2}) \quad (3)$$

$$E_2 = {}^1/_2(H_{bb} + H^U - [(\Delta E^U)^2 + 4(V^U)^2]^{1/2}) \quad (4)$$

$$E_4 = {}^1/_2(H_{bb} + H^U + [(\Delta E^U)^2 + 4(V^U)^2]^{1/2}) \quad (5)$$

These equations were written using $H_{aa} - H_{bb} = \Delta E^U$, $H_{bb} - H_{cc} = \Delta E^L$, and shortening H_{aa} to H^U and H_{cc} to H^L.[21] They can be solved if the relationship between V^U and V^L is known. We are trying to answer this question correctly, but addressing it computationally is a complex and time-consuming problem to implement properly. In the meantime, we have estimated the diabatic energy levels and hence the V^U and V^L values using eqs 6−11, which may be obtained from eqs 2−5

$$\Delta E^U = (E_4 - E_1) - (E_3 - E_2) - \Delta E^L \quad (6)$$

$$V^L = [\{(E_3 - E_1)^2 - (\Delta E^L)^2\}/4]^{1/2} \quad (7)$$

$$V^U = [\{(E_4 - E_2)^2 - (\Delta E^U)^2\}/4]^{1/2} \quad (8)$$

$$H_{bb} = [(E_1 + E_3) + \Delta E^L]/2 \quad (9)$$

$$H^L = (E_1 + E_3) - H_{bb} \quad (10)$$

$$H^U = (E_2 + E_4) - H_{bb} \quad (11)$$

We examine for acceptable solutions by considering the ratio of the proportionality constants for the upper and lower calculated couplings, that is $R = V^U\Delta E^U/V^L\Delta E^L$, because we expect this ratio to be reasonably close to |1|. Only a certain range of ΔE^L values leads to real solutions because of the square roots in eq 7 and 8. At the most negative ΔE^L limit, $H_{bb} = E_2$, $H^U = E_4$, and $R = 0$, while, at the most positive ΔE^L limit, $H_{bb} = E_3$, $H^L = E_1$, and $R = \pm\infty$. Up to three $|R| = 1$ solutions are possible within this range, depending on the relationship between the diabatic energies involved.

The results of these neighboring orbital calculations using the Koopmans-based method for the nine dinitro compounds considered here are shown in Table 3. Only **1,4-PH$^-$** has a three-electron neighboring orbital system (*E_2 SOMO*, and the most stabilized aryl neighboring orbital is filled), and it produces only one real solution for the neighboring orbital system. The others are all one-electron neighboring orbital systems (*E_1 SOMO* and both aryl neighboring diabatic orbitals are virtual) and produce three real solutions. The solutions that have the most positive ΔE^L are easily rejected, because they lead to the monooccupied

(20) (a) Sutin, N. *Prog. Inorg. Chem.* **1983**, *30*, 441−99. (b) Creutz, C.; Newton, M. D.; Sutin, N. *J. Photochem. Photobiol. A* **1994**, *82*, 47−59.

(21) Proper derivations for these equations will appear in a future paper, Nelsen, S. F.; Luo, Y.; Weaver, M. N.; Lockard, J. V.; Zink, J. I. Use of the neighboring orbital model for analysis of electronic coupling in Class III intervalence compounds.

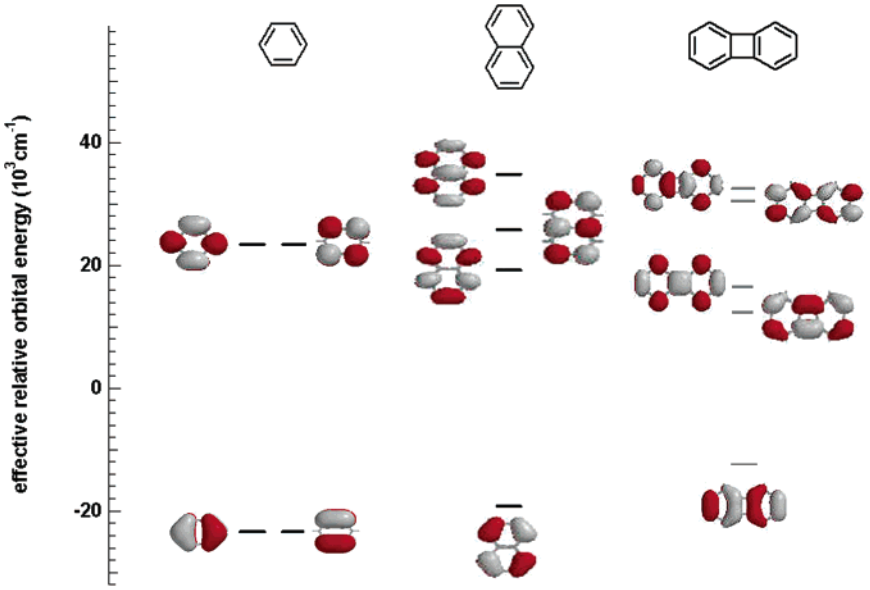

Figure 19. *HOMO* and π virtual orbitals for benzene, naphthalene, and biphenylene.

Scheme 1. *HOMO* and *LUMO* for a Nitro Group, Illustrated for HNO_2

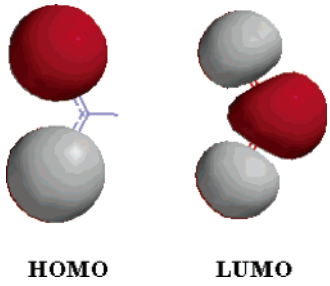

diabatic nitro combination orbital (H_{bb}) lying above both of the virtual aromatic orbitals in energy, which is quite unreasonable. We suggest below that the significant solutions are near the $R = -1$ solutions that are highlighted in Table 3.

The diabatic nitro orbitals of interest for the dinitroaromatic radical anions studied here are symmetric and antisymmetric combinations of the *lumos*, which have a large density at the nitro nitrogen, as illustrated in Scheme 1. The nitro group homo has a node at nitrogen so it will not mix significantly with the aryl π orbitals, while the *lumo* has nodes through the NO bonds and corresponds to π_3 of allyl. The aryl orbitals for three of the bridges used here are shown in Figure 19; the relative size of coefficients makes the orbitals used for neighboring orbital interaction change depending on the substitution pattern, as is examined in detail below. The energies are shown relative to an energy halfway between the *HOMO* and *LUMO*, as is appropriate for these alternate hydrocarbons.

Phenylene-Bridged Cases. The **1,2-** and **1,4-PH-**bridged compounds have very different neighboring orbital interactions, as may be seen from the orbital diagrams for the former in Figure 20 and the latter in Figure 15. **1,2-PH**$^-$ has the NO_2 *LUMO* combination orbitals rather close in energy to the benzene *LUMO* orbitals, and not surprisingly, they are used in the neighboring orbital system, so there is only a single electron in it and E_1 is the *SOMO*. Although the benzene *LUMO* orbitals used by the **1,2-** derivative are of the same energy in benzene itself, they differ by a calculated 12 270 cm^{-1} in the substituted compound. In contrast, although the **1,4-PH** derivative uses the

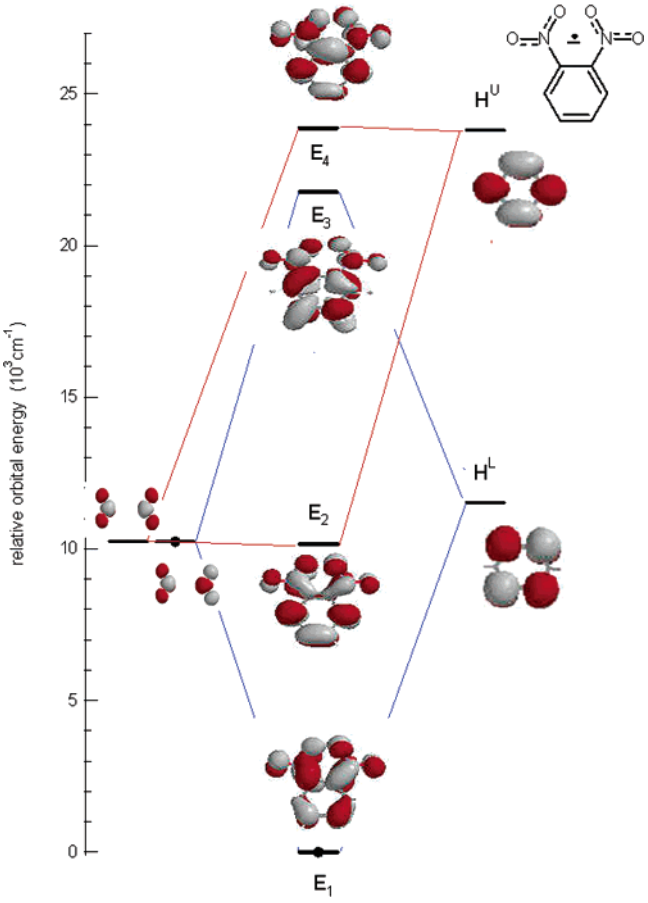

Figure 20. Neighboring orbital energy diagrams for **1,2-PH**$^-$.

same *SS LUMO* (symmetric with respect to planes vertical and horizontal with respect to the drawing shown) as H^U for its neighboring orbital system, the *AA LUMO* is not available because it has a node through C_1 and C_4 so it cannot interact significantly with the nitro combination orbitals. The **1,4-** derivative must by default use the next closest available *A* π orbital as H^L. It is the filled *AS* orbital. This places three electrons in the neighboring orbital system of the **1,4-**derivative.

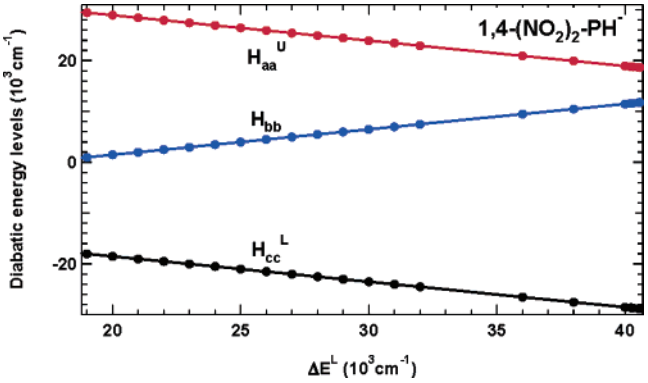

Figure 21. Diabatic energy levels versus ΔE^L for **1,4-PH**$^-$.

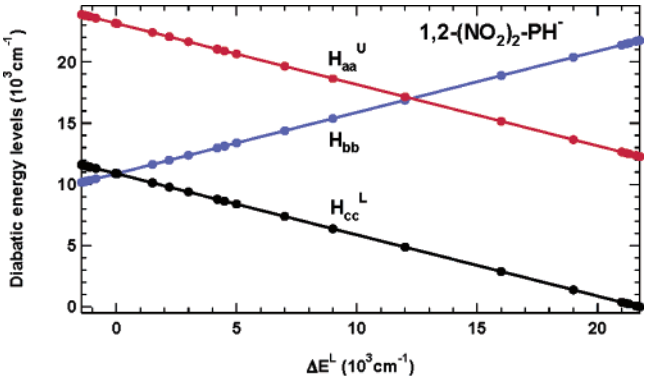

Figure 22. Same as Figure 21 but for **1,2-PH**$^-$.

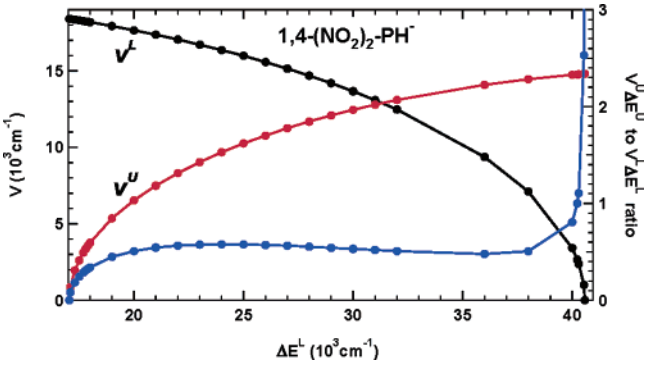

Figure 23. Electronic couplings (left axis) and R values (right axis) versus ΔE^L for **1,4-PH**$^-$.

The difference in the number of electrons in the neighboring orbital systems is important in causing ($H^U - H^L$) for the **1,2-**derivative to be only 26% as large as that for the **1,4-**derivative. Figures 21 and 22 compare the diabatic energy diagrams as a function of ΔE^L for these compounds, and Figures 23 and 24 compare the electronic couplings and R values, while Figures 25 and 26 contain enlargements of Figures 23 and 24 in the region that we suggest is important to consider. R for the **1,4-PH** derivative is extremely insensitive to ΔE^L for almost all the range of real solutions (Figure 23), and only increases to 1 at the high ΔE^L end, where H_{bb} approaches the virtual aryl neighoring orbital. We expect ΔE^L to be rather large for this case because H^L is a filled orbital and H_{bb} is a pair of virtual orbitals. The correct solutions to the neighboring orbital equations are not at the left side of Figure 21, where H_{bb} is near zero relative to the *SOMO* energy. Even though ΔE^L is not well determined, because the large V^L varies little for strongly positive ΔE^L values, its value is well determined for

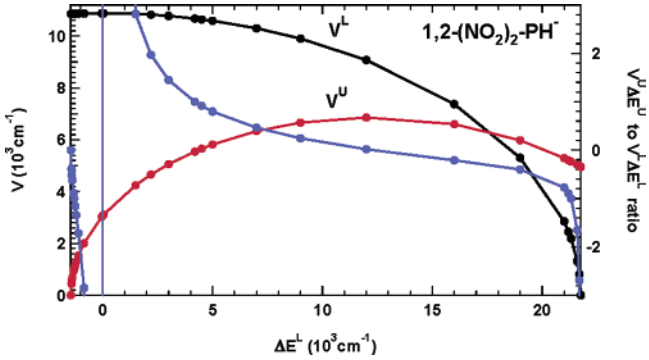

Figure 24. Same as Figure 23 but for **1,2-PH**$^-$.

the neighboring orbital model (as shown in Figure 25). In contrast to the **1,4-** case, R for the **1,2-**derivative is very sensitive to ΔE^L, because R is undefined where H_{bb} crosses H^U (Figure 24). We expect ΔE^L to be negative or small for the **1,2-**derivative because H^L is virtual and H_{bb} is partially occupied. The $\Delta E^L = +4200$ cm^{-1} $R = 1$ solution (Table 3) by definition has H_{bb} that much higher in energy than the virtual H^L, which does not seem as reasonable to us as the $\Delta E^L = -1400$ cm^{-1} solution, which we have chosen in highlighting Table 3 and constructing Figure 20. The same consideration applies to all the other cases, which are also one-electron neighboring orbital systems, so the larger electronic coupling, V^L, is in fact estimated accurately despite uncertainty in what R actually is, because of the nearly flat larger V versus ΔE^L plots in Figure 26 (for similar plots of all the other examples, see the Supporting Information).

Other Bridges. As is documented in full in the Supporting Information, the bridge orbitals that are used in neighboring orbital interactions often change with substitution pattern, choosing the positions of highest coefficient. Thus for the biphenyl bridge, the **2,7-**derivative uses the first and third biphenyl virtual orbitals (the density drawings shown to the right of the four orbital energies in Figure 19), while the **1,8-**derivative uses the second and fourth (density drawings to the left). Similarly, 1,5-dinitronaphthalene uses the first and third virtual orbitals, while the **2,6-**derivative uses the second and third.

A particularly significant aspect of the spectrum of **1,8-BP-** is that, in contrast to the other cases, the lowest energy band region is weak relative to the next higher energy bands instead of being large. This occurs because of the small angle between the coupled dipoles of the aryl−NO_2 units. As pointed out above, the C−N bonds form a 27.7° angle with each other, instead of being well over 90°, like all of the other cases. As discussed in more detail in our work on 2,3-diphenyl-2,3-diazabicyclo[2.2.2]octane,[19] the relative size of the components of the coupled dipoles of the neighboring orbital system depend on the angle their transition dipole moment vectors make with each other, β. The ratio of the lower to the higher energy component transition dipole moments is tan(β/2) for these systems, so the lower energy band greatly predominates when β is near 180°, and only for the low β **1,8-BP**$^-$ case of this series does the higher energy component dominate.

Comparison of Neighboring Orbital and Two-State Electronic Couplings. Figure 27 shows a plot of the larger neighboring orbital V^U value versus the $^1/_2E_{a1}$ value (Table 1) that is equated with the single V value if a simple two-state model is used for these compounds. The general trend is the same, but the numbers are quite different; the intercept is 3800

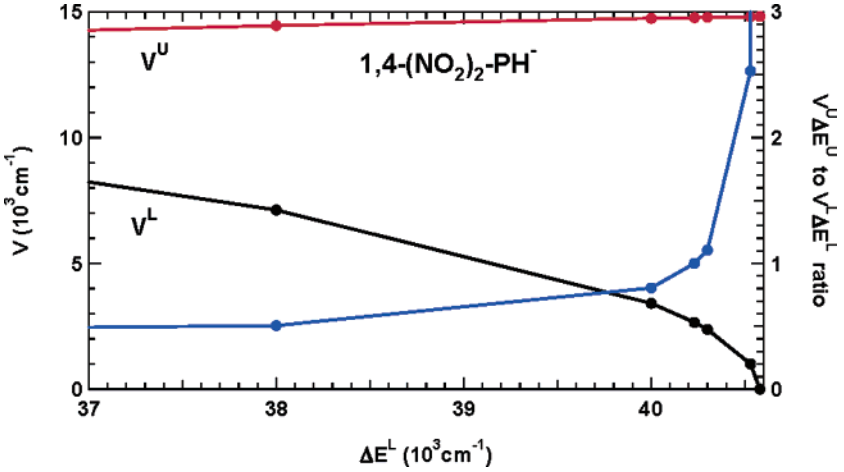

Figure 25. Electronic couplings (left axis) and *R* values (right axis) versus ΔE^L for **1,4-PH**$^-$ near the correct solutions to the neighboring orbital equations.

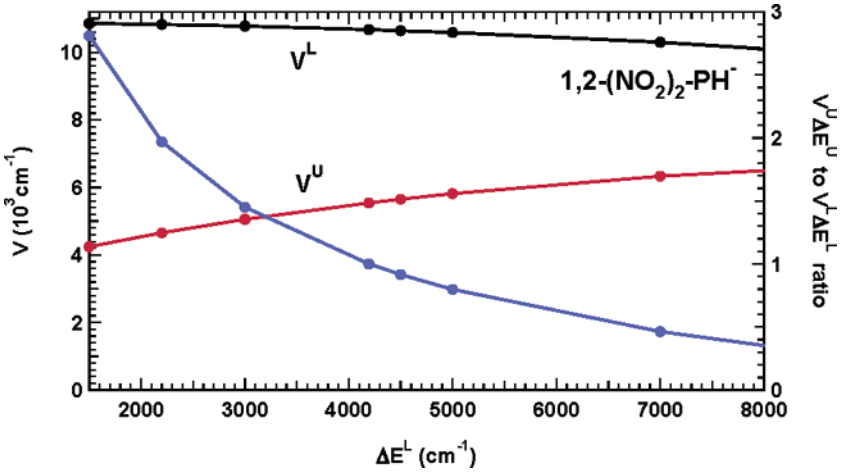

Figure 26. Same as Figure 25 but for **1,2-PH**$^-$.

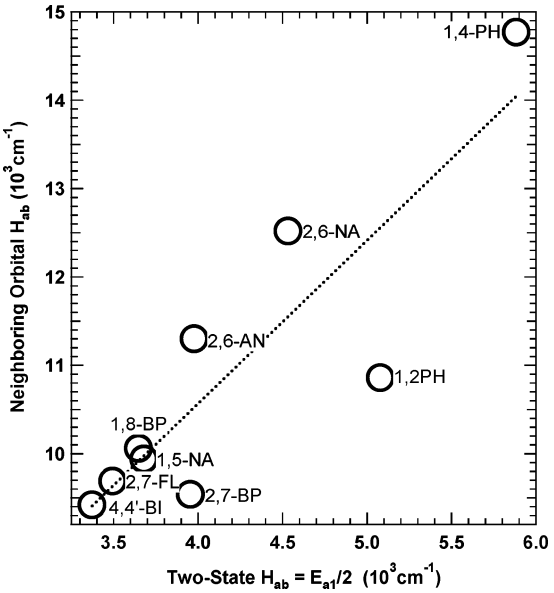

Figure 27. Plot of neighboring orbital larger *V* (Table 1) versus $^1/_2E_{a1}$.

cm^{-1} and the slope is 1.8. The point that falls farthest off the regression line shown, **1,2-PH**$^-$, is for a case that rather clearly has direct overlap between the nitro groups, so the neighboring orbital model may not be a very good approximation for extracting its electronic coupling.

Conclusion

A single-point calculation after artificially emptying (or filling) the *SOMO* for a radical ion by changing the charge employed in the calculation causes the separations between the empty (or filled) orbitals to be usefully close to the type B (or type A) transition energies. The Koopmans-based analysis allows simple depiction of the optical transitions for these species that agree rather well with experimental spectra for the dinitroaromatic radical anions considered here, as well as for other delocalized intervalence compounds, discussed elsewhere. It should be noted that both type A and B bands contribute significantly to these radical anion absorption spectra and that their main features may be predicted without using either configuration interaction or transitions having more complex origin than simple promotions to and from the *SOMO*. The simplicity of the Koopmans-based analysis fits nicely with the simplicity of the neighboring orbital model assumption that only the diabatic bridge orbitals closest in energy to the diabatic charge-bearing unit orbitals need to be considered to estimate electronic couplings. Examination of the orbitals involved in the lowest energy transitions for delocalized intervalence compounds demonstrates that their spectra should not be analyzed using the two-state model. Since allowed optical transitions in these compounds are between orbitals of different symmetry, the transition energies will not be directly related to a single electronic coupling in the molecule. More than one

excited state involving bridge, charge-bearing unit interaction is present so the transition dipole moment for the first band also is not simply related to d_{ab}. The simple two-state model should not be used to analyze delocalized intervalence compounds, and the H_{ab} values derived using it are substantially underestimated. The neighboring orbital model indicates that four adiabatic energies would be required to extract the H_{ab} values for the simplest useful approximation to what is happening in these systems. The $E_1 \rightarrow E_3$ transition is highly forbidden (but sometimes may be visible), while the $E_1 \rightarrow E_4$ transition is essentially always going to be buried under other transitions, making experimental extraction of electronic couplings from optical spectra of these species appear to be unlikely.

Experimental Section

Commercial 1,2-dinitrobenzene (**1,2-PH**) was recrystallized from ethanol.

2,7-Dinitrobiphenylene (2,7-BP). 2,2′-Diiodo-5,5′-dinitrobiphenyl[22] (0.5 g, 1.0 mmol) and activated copper bronze (0.9 g, 14 mmol) in *N*-methyl-2-pyrrolidinone (30 mL) were refluxed under argon with magnetic stirring for 24 h. The mixture was poured into water and filtered, and both the solid and the aqueous phase were extracted with ether. The extract was washed twice with water, dried, and evaporated to dryness. Chromatography on neutral alumina with toluene yielded 2,7-dinitrobiphenylene as fluorescent yellow needles (20 mg, 9%), mp 260 °C (sub.; change in crystal structure at 220°; from toluene/pet.ether; lit.[22] sub. 260 °C); *m*/*z* 242 (M^+); UV (DMF) $\lambda_{max} = 411$ nm, log $\epsilon = 3.9$; ^{1}H NMR (300 MHz; acetone-d_6) δ 7.25 (dd, 2 $H_{4,5}$, $J = 7.7$, 0.6 Hz), 7.75 (dd, 2 $H_{1,8}$, $J = 2.0$, 0.6 Hz), 8.01 (dd, 2 $H_{3,6}$, $J = 7.7$, 2.0 Hz). EPR (radical-anion, DMF) $a_{2N} = 1.42$ G, $a_{2H} = 1.63$ G, $a_{2H} = 0.58$ G, $a_{2H} = 0.50$ G.

(22) Baker, W.; Barton, J. W.; McOmie, J. F. W. *J. Chem. Soc.* **1958**, 2658.

1,8-Dinitrobiphenylene (1,8-BP). 2,2′-Diiodo-6,6′-dinitrobiphenyl (1.0 g, 2.0 mmol, obtained from 2,2′-diamino-6,6′-dinitrobiphenyl by treating its tetrazonium salt with KI) was mixed with 2.3 g of activated copper bronze and heated at 200 °C under argon for 12 h. The mixture was extracted with ether, the solvent evaporated, and the residue chromatographed on silica. Elution with *n*-hexane afforded unreacted diiodo compound, and subsequent elution of the orange band with toluene yielded 1,8-dinitrobiphenylene as orange needles (50 mg, 11%), mp 233−234.5 °C (toluene or acetone); UV (DMF) $\lambda_{max} = 413$ nm, log $\epsilon = 3.5$; ^{1}H NMR (300 MHz; DMSO-d_6) δ 7.24 (dd, 2$H_{3,6}$, $J = 7.2$, 8.4 Hz), 7.29 (d, 2$H_{4,5}$, $J = 7.2$ Hz), 7.42 (d, 2$H_{2,7}$, $J = 8.4$ Hz). ^{13}C NMR δ 122.5, 122.7, 133.4, 139.4, 140.4, 150.9. Constitution was established by ESI-TOF mass spectroscopy; observed *m*/*e* 265.0226, calculated for $C_{12}H_6N_2O_{24}$+Na 265.0225. EPR (radical-anion, DMF) $a_{2N} = 1.94$ G, $a_{2H} = 1.22$ G, $a_{2H} = 1.00$ G, $a_{2H} = 0.20$ G.

Acknowledgment. We thank financial support of this work from the National Science Foundation under Grant CHE-0240197 (S.F.N.) and from Fundação Para a Ciência e Tecnologia through its Centro de Química Estrutural (J.P.T.). We thank Frank Weinhold (UW) for showing us how to obtain the band intensities for Koopmans-based transitions using his NBO program.

Supporting Information Available: TD-DFT and NAG/DAG calculation comparisons (like Table 1) for **1,5-NA**$^-$ and **1,5-NA**$^-$ (both 6-31+G* and 6-31G* basis sets) and for **2,7-BP**$^-$ and **1,8-BP**$^-$. Neighboring orbital density drawings (like Figure 20) for these compounds, **4,4′-BI**$^-$, and **2,7-M$_2$FL**$^-$. Neighboring orbital solution plots (like Figures 21−26) for these compounds and **2,6-AN**$^-$. This material is available free of charge via the Internet at http://pubs.acs.org.

JA051178U